A major purpose of the Technical Information Center is to provide the broadest dissemination possible of information contained in DOE's Research and Development Reports to business, industry, the academic community, and federal, state and local governments.

Although a small portion of this report is not reproducible, it is being made available to expedite the availability of information on the research discussed herein.

LA-UR-84-2735

CONF-840911 8--3

Los Alamos National Laboratory is operated by the University of California for the United States Department of Energy under contract W-7405-ENG-36

TITLE POTENTIAL PERFORMANCE BENEFITS OF ADVANCED COMPONENTS AND MATERIALS RESEARCH

AUTHOR(S) Donald A. Neeper
Robert D. McFarland
James C. Hedstrom
Gloria S. Lazarus

SUBMITTED TO Passive and Hybrid Solar Energy Update
Alexandria, Virginia
September 5-7, 1984

Los Alamos Los Alamos National Laboratory
Los Alamos, New Mexico 87545

POTENTIAL PERFORMANCE BENEFITS OF ADVANCED COMPONENTS AND MATERIALS RESEARCH*

D. A. Neeper, R. D. McFarland, J. C. Hedstrom and G. S. Lazarus
Los Alamos National Laboratory
Los Alamos, New Mexico 87545

ABSTRACT

This paper reports work in progress to identify the potential impact of new components and materials on the energy savings, comfort, or utility of buildings. As of this writing, three new items have received preliminary examination. Wallboard containing phase change material (PCM) for thermal storage appears very promising. PCM combined with sensible storage can significantly reduce the storage volume in water walls, liquid convective diodes, and hybrid heating systems. Aerogel window glazings with present aerogel properties appear to be superior to existing materials only in applications with low insolation or very cold temperatures, but an increase in optical transmission of the material could lead to a glazing that is superior in all climates with significant winters.

PCM WALLBOARD

Current design guidelines [1] recommend that direct gain heating utilize a thermal storage area of radiatively coupled masonry that is 6 times the glazing area and 4 in. thick. If the glazing area is large, so as to provide a large solar savings fraction (SSF), it is difficult in design to provide the recommended area of radiatively coupled mass. Furthermore, mainstream builders find the use of extensive masonry to be a departure from their normal construction practice. The question is this: Can the large areas of wallboard that ordinarily occur in a residential building be utilized for convectively coupled thermal storage? So-called sun-tempered buildings that utilize the heat capacity of ordinary gypsum wallboard have thermal storage that limits the glazing area, and, hence, limits the SSF to less than 25%, even in a strong solar climate such as Albuquerque.

The passive program is attempting to develop a wallboard material that could contain 20% phase change material (PCM) by weight [2]. For a 5/8-in.-thick board, this could provide up to 34 Btu/ft^2 of latent heat storage, in addition to sensible storage that is comparable to that of ordinary gypsum board. As an example, we consider a building with 1200 ft^2 of floor area, 300 ft^2 of direct gain aperture, and the recommended 1800 ft^2 of concrete storage. For a temperature swing of 10°F, the diurnal heat capacity of the concrete is 170,000 Btu if radiatively coupled, and 79,000 Btu if convectively coupled [3]. Alternatively, this building could have no masonry but a latent storage of 122,000 Btu in 3600 ft^2 of wallboard. This is sufficient storage for a significant SSF if the convective coupling to the PCM board is adequate.

To test the adequacy of convective coupling, we consider a model house with 1200 ft^2 of floor area and a heating load of approximately 7200 Btu/°F day in addition to the load of the solar aperture. In addition to varying amounts of convectively coupled wallboard, this house has light-colored wallboard (absorptance 0.3) with triple the aperture area, which is illuminated by the aperture. The illuminated wallboard has a convective heat transfer coefficient (U) of 1.5 Btu/ft^2 h °F. We utilize the climate of Albuquerque because it has cold nights and strong insolation so that the SSF is sensitive to thermal storage. The PCM wallboard used in these calculations has a latent heat of 21 Btu/ft^2 (or about 61% of the projected maximum value of 34 Btu/ft^2). Both the PCM wallboard and the gypsum wallboard have 0.677 Btu/ft^2 °F of sensible heat capacity.

Figure 1 shows the SSF as a function of U-value at the surface of the convectively coupled mass for different aperture areas (A_c). The

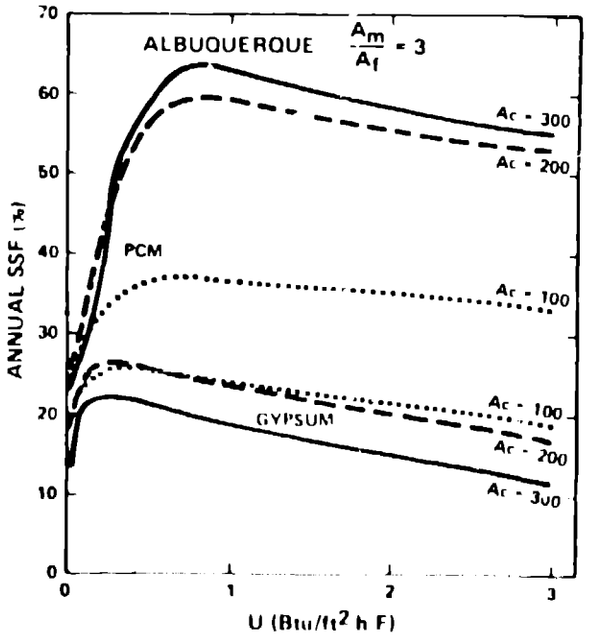

Fig. 1. SSF as a function of U value at the surface of the convectively coupled mass. A_c is the aperture area in ft^2.

*Work performed under the auspices of the US Department of Energy, Office of Solar Heat Technologies.

convectively coupled mass area is 3 times the floor area (A_m/A_f = 3); 100 ft^2 of aperture is an upper limit for a sun tempered house. Indeed, in the lower three curves for ordinary gypsum wallboard, one can see that the SSF decreases as A_c is increased. An increase in A_c admits more solar radiation to the house. However, because the storage is inadequate, this added energy must be vented, while the increased aperture increases the energy loss at night, leading to more use of auxiliary energy and a lower SSF. The PCM wallboard dramatically increases the SSF up to an aperture size of 200 ft^2. At this point, again increasing the aperture area to 300 ft^2 increases the SSF only slightly, because the storage is nearly fully utilized at A_c = 200 ft^2.

Figure 1 shows that, for A_m/A_f = 3, the maximum SSF occurs near U = 0.75, with a slight decrease above this value and a dramatic decrease below U = 0.5. The naturally occurring U-value at an extended surface is in the range 1.0-1.5 so that it appears that natural convective coupling will be nearly optimal. However, much of the internal surface area of residences is in rooms that may be separated from the direct gain zone by doorways. Consider a room containing 600 ft^2 of wallboard with U = 1.5. If this room is connected to a direct gain zone that is 3°F warmer by a doorway 6.67 ft high by 2.67 ft wide, the thermal resistance of the doorway [4] will cause the effective U-value of the wallboard to be approximately 0.4. As shown in Figure 1, this would induce a significant performance penalty. Thus, the use of PCM wallboard should be accompanied by large interzone openings (which is good passive design practice anyway). When large openings are impractical, the interzone convection problem can probably be overcome by operation of the fan of a forced-air auxiliary furnace during strong solar days.

Figure 2 shows SSF vs the ratio of convectively coupled mass area to floor area. The PCM curve for A_c = 100 has become horizontal above A_m/A_f = 2, indicating that additional thermal storage would have no effect. The PCM curves for A_c = 200 ft^2 and A_c = 300 ft^2 both slope upward at A_m/A_f = 3, indicating that more storage would be beneficial. Because A_m/A_f = 3 is roughly a practical upper limit, a thicker wallboard could be used.

As a final point, we note in Fig. 1 that at A_c = 200 ft^2, A_m/A_f = 3, the SSF is between 55 and 60%. For comparison, we note that currently recommended direct gain design [1] for this load and aperture area (LCR = 35) should have an SSF of 55%. Thus, a designer using PCM wallboard should often be able to achieve the same energy savings that are possible with extensive masonry. In addition, the PCM wallboard may offer advantages for ventilative cooling. From this preliminary part of our study, we conclude that this material offers new opportunities for both retrofit and new construction.

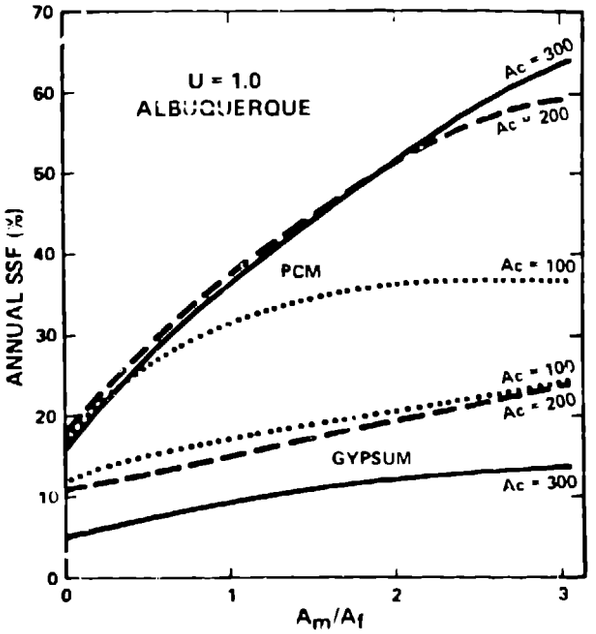

Fig. 2. SSF as a function of the ratio of convectively coupled mass area to floor area.

COMBINED PCM-SENSIBLE THERMAL STORAGE

Phase change materials offer the possibility for thermal storage in much less volume than is required by water or masonry. However, one difficulty with PCM has been in obtaining adequate heat transfer at the surface of the encapsulated material. We note that modules of encapsulated PCM could, in principle, be immersed in a water storage tank. This should enable a great reduction in tank volume, while permitting better heat transfer to the PCM than could be achieved if the circulating fluid were air.

The possibility of reduced storage volume is particularly attractive for prefabricated water walls and for indirect systems in which the storage is not illuminated by the sun. For example, PCM capsules might be used in the storage reservoir of a convective diode [5], or in the distributed storage tanks of a hybrid (active charge, passive discharge) heating system, which is of particular interest for retrofits. In a Trombe wall application, Bourdeau [6] found that the PCM would permit a thinner wall, but it would not provide significantly greater energy savings than a similar wall with adequate sensible storage. Likewise, if PCM is combined with sensible storage, we have found the effect to be reduced storage volume at the same energy savings. With computer modeling, we have studied the effects of combined PCM-water storage in a hybrid system in which a remote vapor-generating collector heated a storage tank, which in turn passively heated a building in Albuquerque. However, our results should be valid for almost any system that employs combined storage.

Heat transfer parameters are normalized to collector area (ft_c^2). The building load is 2 Btu/h ft_c^2 °F (LCR = 48); the storage-to-room heat transfer coefficient is 4 Btu/h ft_c^2 °F. The PCM is assumed to have a reversible melting temperature of 81°F, a latent heat of 82 Btu/lb, a heat capacity when solid of 0.34 Btu/lb °F, and a heat capacity when liquid of 0.53 Btu/lb °F. These properties approximately represent $CaCl_2 \cdot 6H_2O$. We assume that the PCM is in perfect thermal contact with the water. Although this assumption needs to be examined, we note that the thermal resistance between the water and the PCM is likely to be much smaller than the thermal resistance between the storage tank and the room air.

Figure 3 shows SSF as a function of total storage mass (M_w = mass of water; M_p = mass of PCM). The lowest curve is for water storage only with no PCM. A good passive system often has sensible storage equivalent to 30-45 lb water per ft^2 of collector, and we notice in Fig. 3 that the SSF increases only slightly for storage greater than 45 lb water ft_c^2. The highest curve is for PCM only, with no water but retaining the hypothetically perfect heat transfer to the PCM. The intermediate curves of Fig. 3 represent 1, 5, and 15 lb/ft_c^2 of water in combination with varying amounts of PCM.

In Figure 4 SSF is plotted as a function of a reduced PCM mass, M_p^*, which represents the hypothetical mass of PCM with latent heat only (no sensible heat capacity), that would result in the same diurnal storage as a combined system or a water-only system. The upper horizontal scale of Fig. 4 is the reduced water mass M_w^*, which represents the mass of water in a system that contains no PCM. The reduced masses are defined by Eq. (1).

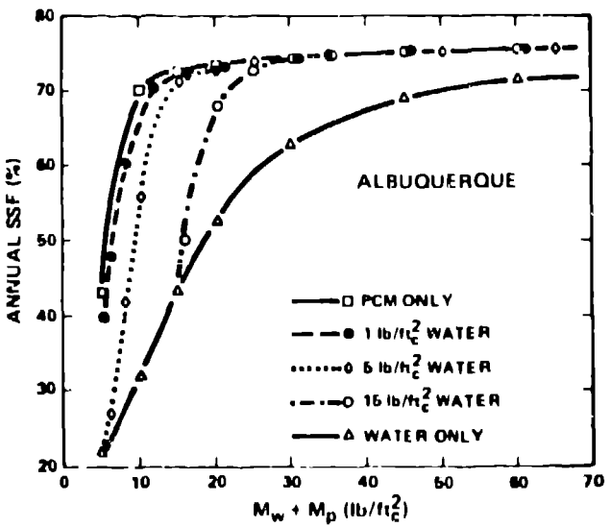

Fig. 3. SSF as a function of total storage mass for various amounts of water in lb/ft_c^2.

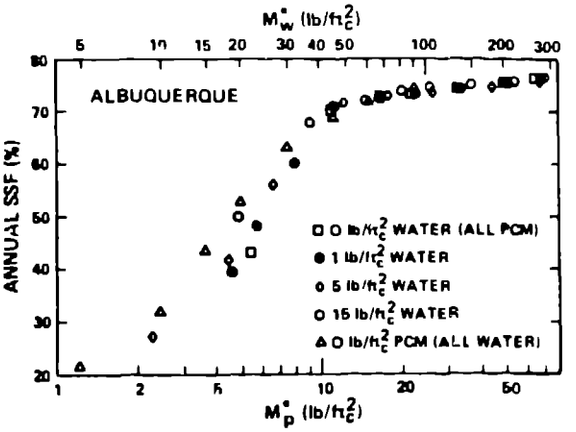

Fig. 4. SSF as a function of the reduced mass of PCM (lower scale) or reduced mass of water (upper scale).

$$LM_p^* = C_w \Delta T M_w^* = (L + C_p \Delta T) M_p + C_w \Delta T M_w \quad . \tag{1}$$

In Eq. (1), L is the latent heat of the PCM, C_p is the heat capacity of the PCM, C_w is the heat capacity of water, ΔT is the assumed diurnal temperature swing of the storage that contains M_p mass of PCM and M_w mass of water. ΔT was treated as a curve-fitting parameter chosen so as to define a common value of M_p^* at SSF = 70% for the curves representing 1, 5, and 15 lb/ft_c^2 water. (In normalizing the curves, the specific heat of the solid PCM was used.) A ΔT of 20°F resulted. This seems physically reasonable, but has not been checked against the actual daily variation of storage temperature in the computer model. Figure 4 shows that all of the curves of Fig. 3 follow the same functional form. This demonstrates that PCM and sensible material can be used interchangeably.

From Eq. (1) we can derive a general expression for the mass of a combined storage system, relative to the mass M_w^* of an all-water system with the same energy savings.

$$(M_p + M_w)/M_w^* = X + (1 - X) M_w/M_w^* \tag{2}$$

$$X = C_w \Delta T/(L + C_p \Delta T) \quad . \tag{3}$$

Eq. (2) shows how the total mass of a combined storage system (relative to that of all water storage) varies as the water fraction is varied. If the PCM is calcium chloride hexahydrate, the minimal possible storage mass is about one-fourth of the mass of an all-water system. Because the average density of encapsulated PCM might be close to the density of water, the reduction in storage volume will be close to the reduction in storage mass.

We conclude that for a given collector area and building load, the annual energy savings appear to be a unique function of the average ener-

gy stored per day, independent of whether the storage is latent (occurring at one temperature) or sensible (occurring over a diurnal temperature swing), or a combination of both. This means that the energy savings provided by one pound of calcium chloride are almost identical to the savings provided by 4.44 pounds of water. This reduction in storage volume could be an important benefit for water walls and for hybrid systems in retrofit applications. Combining encapsulated PCM with water should provide good heat transfer to the PCM, although this remains to be examined. In effect, the previous section of this paper demonstrated a similar reduction of storage volume in which the masonry of a direct gain system was replaced by a smaller volume of gypsum combined with PCM. In that case, the necessary improvement in heat transfer was achieved by greatly increasing the area of the storage material to comprise all interior wall and ceiling surfaces of the building.

EVALUATION OF THERMAL GLAZINGS[7]

As demonstrated by hourly calculations of Harrison and Barakat [8], the average energy gain (or loss) per unit area of a window can be represented by

$$\bar{Q} = \bar{F} \cdot \bar{H} - \bar{U} \cdot \overline{\Delta T} \quad . \tag{4}$$

In Eq. (4) $\bar{F}$ is the average solar heat gain coefficient, which is the sum of the transmitted solar radiation and the inwardly conducted portion of the solar radiation that is absorbed in the glazing. $\bar{H}$ is the average radiation on the plane of the glazing, $\bar{U}$ is the average loss coefficient, and $\overline{\Delta T}$ is the average indoor/outdoor temperature difference. Eq. (4) can be arranged to give an average performance factor (or efficiency), $\bar{\eta}$:

$$\bar{\eta} = \bar{Q}/\bar{H} = \bar{F} - \bar{U}(\overline{\Delta T}/\bar{H}) \quad . \tag{5}$$

Eq. (5) permits comparison of the thermal performance of various glazings as linear plots of $\bar{\eta}$ vs $(\overline{\Delta T}/\bar{H})$, in which for each glazing $\bar{F}$ becomes the vertical intercept of the line, $\bar{U}$ becomes the negative slope of the line, and $(\overline{\Delta T}/\bar{H})$ is a single parameter that represents climate and window orientation for all glazings. In truth, $\bar{F}$ will be somewhat dependent upon climate and orientation because the average angle of incidence will vary with latitude and cloudiness. However, for a vertical glazing, the diffuse sky and ground-reflected radiation has a constant effective incidence angle of 60°, and at a latitude of 40°, the winter monthly average angle of incidence for beam radiation on a vertical south surface is between 38° and 60° [9]. Thus, we expect that a suitable value of $\bar{F}$ for a winter season might be calculated using an average angle of incidence between 40° and 60°. Indeed, we found that $\bar{F}$ for double glazing calculated from a single average incidence angle of 55° agreed with the value of $\bar{F}$ in Ref. [8], derived from hourly calculations. Therefore, we used a seasonal average incidence angle of 55° in all of our calculations, although it may have been slightly more accurate to use a 60° angle for north-facing glazings.

Using the method of Rubin [10], we have calculated $\bar{F}$ for ordinary windows and for windows with aerogel between two layers of glass. In the absence of detailed optical information, we made the rough approximation that radiation entering aerogel is either transmitted by the beam or perfectly backscattered, which is optically equivalent to a plane reflection. The normal-incidence transmittance and thermal conductivity of aerogel were taken from Ref. [11]. (At an incidence angle of 55°, the optical path length in a 20-mm slab of material is 34.9 mm. For this path length, the transmittance of aerogel given in Ref. [11] was extrapolated according to an exponential that closely fits the data.)

Figure 5 presents the efficiency at 55° incidence of a single glazing of float glass (SG), a double glazing of float or low-iron glass (DG), a window with 5 mm (0.197 in.) of aerogel between glass layers (5A), a similar window with 20 mm (0.787 in.) of aerogel (20A), a triple-pane glazing with an internal heat mirror layer (g-ph-g), and a quad-pane glazing with two internal high-transmission polyester layers (g-a-a-g). The spacing of layers in all multiple glazings except the aerogel windows was assumed to be 1/2 in. Properties of the heat mirror and quad-pane glazings were taken from Ref. [12], which simply states that non-normal incidence angles were used. Also shown in Fig. 5 is the line representing the heat loss from an R18 insulated wall that does not absorb solar radiation (a white wall), and a line labeled "20A FUTURE?" that represents a proposed performance goal for aerogel windows discussed at the conclusion of this section of this report. The arrows in Fig. 5 mark values of $\overline{\Delta T}/\bar{H}$ (°F ft^2 h/Btu) for south vertical surfaces at various cities for the season November-March. The lines labeled DG, 5A, and 20A are pairs, with the upper line of each pair representing 1/8 in. low-iron glass and the lower line representing 1/8-in. float glass.

Figure 5 permits an easy comparison of the relative benefits of the various glazings. A positive efficiency means that the window gains more energy than it loses during the season; a negative efficiency indicates a net loss. At any particular value of $\overline{\Delta T}/\bar{H}$, that window (or wall) with the highest efficiency has the highest energy savings. The net energy gained or lost by the window during the season is the product of the average efficiency, $\bar{\eta}$, with the appropriate $\bar{H}$ for the climate and orientation in question. Note that double glazing, both aerogel windows, and the heat mirror glazing have approximately the same energy performance at $\overline{\Delta T}/\bar{H} = 1.05$. For a south window in Albuquerque ($\overline{\Delta T}/\bar{H} = 0.39$), double glazing gives the best performance. However, one can see that south double glazing in Buffalo ($\overline{\Delta T}/\bar{H} = 1.79$) loses slightly more energy than an R18 wall, and the quad-pane window has the highest energy savings. For north-facing surfaces, which usually have $\overline{\Delta T}/\bar{H} > 3$, the 20A glazing has the highest efficiency of all the present glazings, but it is not more energy efficient than the insulated wall in all locations.

Table 1 presents the net seasonal energy balance for both north- and south-facing surfaces.

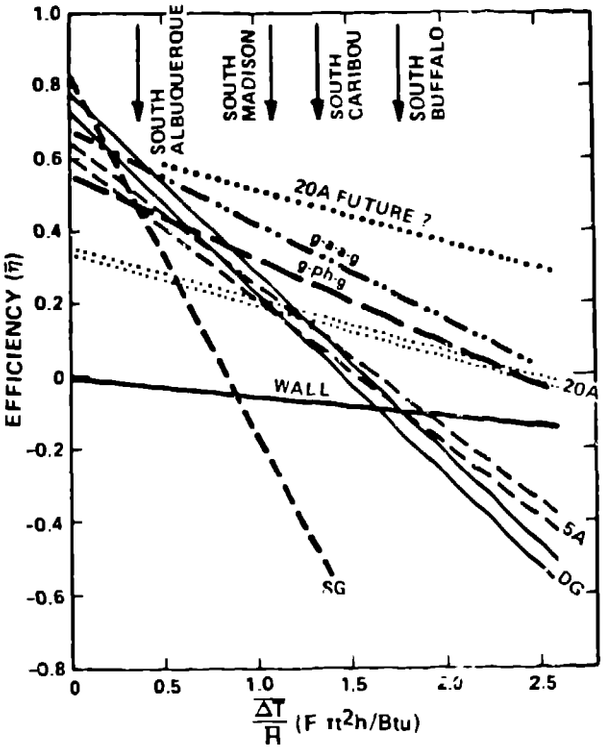

Fig. 5. Average efficiency of various windows as a function of average climate and orientation parameter for the period November-March.

For south-facing surfaces, aerogel windows of the present material do not offer a significant energy advantage over those that can be obtained with currently marketed materials, although the aerogel may in the future prove to have advantages in thickness or durability. For a north-facing window, the 20 mm aerogel clearly gives the best performance. In severe climates, the north-facing aerogel may save approximately 10,000 Btu/ft^2 per year more than its nearest glazing competitor.

Although the 20A glazing does not have the best energy efficiency in all climates, one can see in Fig. 5 that it is the glazing with the highest R-value, or lowest slope of the line. One could increase the R-value (decrease the slope of the line) of the multiple glazings by adding more internal layers to those glazings. However, this would also lower their solar heat gain, or $\bar{F}$, represented by the vertical intercepts of their lines. A truly superior glazing could be formed by increasing the solar heat gain ($\bar{F}$) of the 20A glass-aerogel sandwich from its present range near 35% to approximately 65% at 55° incidence. In Fig. 5, this would result in the line labeled "20A FUTURE?," which is also represented by a corresponding entry near the bottom of Table 1. Such a glazing would be superior to all of the other glazings considered here in all applications with $\Delta T/H$ greater than 0.39, that is, in all climates and orientations less favorable than that of a south-facing surface in Albuquerque. It would have winter energy savings greater than those of the R18 wall in all climates and all orientations. We have assumed that the normal-incidence optical transmission of a 20 mm thickness of present-day aerogel is 59% [11]. The encapsulating layers of glass, when combined with the aerogel, cause the solar heat gain ($\bar{F}$) of the 20A window at 55° incidence to be approximately 35%. The desired increase of $\bar{F}$ to 65% would require that the normal-incidence optical transmission of 20 mm of aerogel be increased from 59% to approximately 88%. The researchers may be able to determine if this is a reasonable goal.

It must be emphasized that the information in Table I and Fig. 5 is based upon many assumptions that have not yet been adequately tested. It is not certain that a 55° average angle of incidence is appropriate for the climates and glazings considered. It was used because it permitted agreement with the detailed calculations of Ref. [8] for double float glass, and because it was within the physically reasonable range. It is not clear that the lines of Fig. 5 for the heat mirror and quad-pane glazings correspond to a 55° incidence angle. Our treatment of aerogel as having no absorption and only perfect backscattering may not be accurate. Thus, our calculations are intended merely to permit rough comparisons, and are subject to revision as we obtain better optical data and utilize more refined methods. Numbers presented here are intended for use in programmatic planning, not for input to other systems analysis.

ACKNOWLEDGMENTS

We appreciate discussions with Michael Rubin and Craig Christensen that made the glazing evaluation possible.

REFERENCES

1. Balcomb, J. D., Jones, R. W., McFarland, R. D., and Wray, W. O., Passive Solar Heating Analysis, ASHRAE, Atlanta, Georgia, 1984.

2. Salyer, Ival, private communication.

3. Balcomb, J. D., "Heat Storage and Distribution Inside Passive Solar Buildings," Los Alamos National Laboratory report LA-9594-MS (May 1983)), p. 41.

4. Ibid., p. 59.

5. Suggested by T. Maloney of One Design, Inc.

6. Bourdeau, Luc E., "Study of Two Passive Solar Systems Containing Phase Change Materials for Thermal Storage," Proc. Fifth National Passive Solar Conference, Amherst, Massachusetts, October 19-26, 1980, p. 297.

7. This evaluation considers the energy gains or losses of a window, with room temperature assumed constant so that only the glazing

TABLE 1

NET ENERGY TRANSMITTED BY VERTICAL WINDOWS
NOVEMBER-MARCH (kBtu/ft^2)*

	South				North			
	Albuquerque New Mexico	Madison Wisconsin	Caribou Maine	Buffalo New York	Albuquerque New Mexico	Madison Wisconsin	Caribou Maine	Buffalo New York
$\overline{\Delta T}/\overline{H}$ (°F ft^2 h/Btu)**	0.39	1.09	1.34	1.79	3.51	5.72	6.80	4.76
Single float glass	116.4	-35.9	-66.3	-73.4	-75.6	-132.6	-154.5	-113.8
Double glass								
float	139.6	26.7	7.8	-12.8	-29.2	-58.3	-69.7	-48.3
low-iron	153.1	34.2	14.7	-8.7	-27.7	-56.9	-68.4	-46.7
5 mm aerogel								
float	116.8	24.2	8.9	-8.7	-22.8	-46.1	-55.3	-38.0
low-iron	127.3	30.0	14.2	-5.5	-21.6	-45.0	-54.2	-36.8
20 mm aerogel								
float	72.0	25.4	18.6	6.0	-4.8	-13.3	-16.7	-10.2
low-iron	77.6	28.5	21.5	7.7	-4.2	-12.7	-16.1	-9.6
+Glass-heat mirror-glass (g-ph-g)	121.2	43.5	32.3	10.9	-7.4	-21.2	-26.8	-16.1
+Glass-poly-poly-glass (g-a-a-g)	150.3	56.5	43.1	16.2	-7.1	-22.8	-29.2	-16.9
20A FUTURE?	154.6	71.1	60.7	30.7	4.2	-4.6	-8.4	-0.9
++R18 Opaque white wall	-5.6	-8.7	-9.9	-7.7	-5.6	-8.7	-9.9	-7.7

* Assumed room temperature 68°F.
** Anisotropic sky model. Ground reflectance 0.3.
\+ Net energy obtained using shading coefficients and U-values for half-inch gap widths from Rubin [12]. Glass is float glass, heat mirror is single-coated 4 mil polyester, poly is 4 mil polyester with both sides antireflective coated.
++ Shown for comparison with windows.

properties influence the evaluation. A different type of evaluation, considering the window size, building load, and thermal storage, is in progress by Craig Christensen.

8. Harrison, S. J., and Barakat, S. A., ASHRAE Trans. 89, Part 1A, Paper 2735 (1983).

9. Duffie, J. A., and Beckman, W. A., Solar Engineering of Thermal Processes, New York: John Wiley and Sons, 1980, p. 191.

10. Rubin, Michael, "Solar Optical Properties of Windows," Int. J. Energy Research 6, 123 (1982).

11. Rubin, Michael, and Lampert, Carl M., "Transparent Silica Aerogels for Window Insulation," Solar Energy Materials 7, 393 (1983), also distributed as LBL-14462.

12. Rubin, Michael, and Selkowitz, Stephen, "Thermal Performance of Windows Having High Solar Transmittance," Proceedings of the Sixth National Passive Solar Conference, Portland, Oregon, September 8-12, 1981, p. 141.